JOURNAL OF ELECTROMAGNETIC ENGINEERING AND SCIENCE, VOL. 16, NO. 3, 169~181, JUL. 2016

http://dx.doi.org/10.5515/JKIEES.2016.16.3.169
ISSN 2234-8395 (Online) · ISSN 2234-8409 (Print)

Design, Analysis, and Equivalent Circuit Modeling of Dual Band PIFA Using a Stub for Performance Enhancement

Jawad Yousaf[1] · Hojin Jung[2] · Kwangho Kim[1] · Wansoo Nah[1,*]

Abstract

This work presents a new method for enhancing the performance of a dual band Planer Inverted-F Antenna (PIFA) and its lumped equivalent circuit formulation. The performance of a PIFA in terms of return loss, bandwidth, gain, and efficiency is improved with the addition of the proposed open stub in the radiating element of the PIFA without disturbing the operating resonance frequencies of the antenna. In specific cases, various simulated and fabricated PIFA models illustrate that the return loss, bandwidth, gain, and efficiency values of antennas with longer optimum open stub lengths can be enhanced up to 4.6 dB, 17%, 1.8 dBi, and 12.4% respectively, when compared with models that do not have open stubs. The proposed open stub is small and does not interfere with the surrounding active modules; therefore, this method is extremely attractive from a practical implementation point of view. The second presented work is a simple procedure for the development of a lumped equivalent circuit model of a dual band PIFA using the rational approximation of its frequency domain response. In this method, the PIFA's measured frequency response is approximated to a rational function using a vector fitting technique and then electrical circuit parameters are extracted from it. The measured results show good agreement with the electrical circuit results. A correlation study between circuit elements and physical open stub lengths in various antenna models is also discussed in detail; this information could be useful for the enhancement of the performance of a PIFA as well as for its systematic design. The computed radiated power obtained using the electrical model is in agreement with the radiated power results obtained through the full wave electromagnetic simulations of the antenna models. The presented approach offers the advantage of saving computation time for full wave EM simulations. In addition, the electrical circuit depicting almost perfect characteristics for return loss and radiated power can be shared with antenna users without sharing the actual antenna structure in cases involving confidentiality limitations.

Key Words: Equivalent Circuit (EC), Equivalent/Electrical Circuit Model (ECM), Planer Inverted-F Antenna (PIFA), Rational Approximation (RA), Vector Fitting (VF).

I. INTRODUCTION

Multiband small-size Planer Inverted-F Antennas (PIFAs) are designed to compensate the reduction in size and space of modern era mobile phones. Modern portable cellular devices also require increased operational bandwidth for the installed antennas, preferably in several bands [1, 2]. Previously, shaping and tilting of the antenna structure was proposed to increase the operational characteristics of multiband antennas [3]. However, modern techniques for enhancement of an antenna's perfor-

Manuscript received April 1, 2016 ; Revised June 20, 2016 ; Accepted July 9, 2016. (ID No. 20160401-011J)
[1]Department of Electronic and Electrical Engineering, Sungkyunkwan University, Suwon, Korea.
[2]Advanced H/W R&D Team 1, Mobile Communication Division, Samsung Electronics Co. Ltd., Suwon, Korea.
[*]Corresponding Author: Wansoo Nah (e-mail: wsnah@skku.edu)

mance (e.g., VSWR, return loss, etc.) include E-shaped [4] and L-shaped [5] slitting in the antenna structure, using a pin instead of a plate for shortening [6, 7], adjustment of the space between the feed and short [7, 8], matching circuits [9], meandering [10], optimum height of the radiating patch [7], size of the ground plane [6, 7], broadband circular patches [6], and ground plate slotting [11] . The increase in the bandwidth of the antennas is proportional to the antenna volume. Antenna volume is highly dependent upon the radiating element and ground plane as these elements enclose the forming strong electric field area. In [12], the author proposes that antenna volume can be increased by shifting the radiating patch away from the ground plane. The shifting of the radiating element enhances the antenna bandwidth because of reduced ground area [12].

PIFAs are usually installed at the bottom end of a mobile phone to provide the maximum isolation to the data processing module and to control the specific absorption rate (SAR) magnitude. Most modern cell phones have a structure with a bottom interface connector (IC) used for data exchange and power purposes. The IC is located in close proximity to the antenna and its metallic structure causes the degradation of various antenna performance metrics. It particular, it degrades the antenna's radiation parameters (gain and efficiency), return loss, and bandwidth in lower bands, such as GSM 850 and GSM 900. In this study, a method is proposed for improving dual band PIFA performance using an open stub in the vicinity of the metallic IC. The addition of an open stub away from the ground plane enhances the antenna volume, which results in incremental improvements of various performance metrics. A gradual increase in the length of the introduced open stub in the PIFA radiating structure shows an enhancement of up to 4.6 dB in return loss, 17% in bandwidth, 1.8 dBi in gain, and 12.4% in the efficiency of the antenna. The experimental results of the proposed antenna structure are in good agreement with the simulation results.

Equivalent circuit models (ECMs) of antennas are developed for their time domain analysis [13], better understanding of their resonance phenomena, and for systematic antenna designs from the equivalent circuit. The equivalent circuit of simple antenna structures with one resonance point can be derived in the form of transmission line models [14–16], frequency independent lumped element resonant structures [17, 18], and physics-based compact lumped structures using the partial element equivalent circuit (PEEC) technique [19]. However, it is difficult to formulate equivalent circuits for complex antenna structures with multiple resonances. The PEEC technique provides the SPICE equivalent lumped element circuit of antennas but it results in a large number of lumped elements in the circuit [19]. In [20], the author derives a dual band PIFA equivalent circuit using radiated and balanced mode analysis, [21] presents a single band PIFA equivalent circuit based on equivalent modes, and [22] shows that a single/dual band high Q_PIFA equivalent circuit can be derived using an RLC resonator. To the best knowledge of these authors, the literature only contains PIFA electrical circuit modeling techniques [19–22] for simple PIFA geometries having single/dual band operational characteristics. Cabedo et al. [23] present the electrical modeling of a pentaband PIFA (simple geometry) based on RLC resonators. There is a paucity of literature on equivalent circuit modeling of multiband PIFAs with complex geometries.

The present work also presents a simple way to derive lumped equivalent circuits for multiband PIFAs. The lumped equivalent circuit of the designed dual band PIFA is derived from the rational approximation of its frequency domain response [24]. The frequency response (scattering/admittance parameters) of the antenna is obtained in tabular form through full wave electromagnetic simulation as well as from measurements of the fabricated antenna model. The tabular data is approximated to a rational function using the vector (pole fitting) technique [24, 25]. Subsequently, the lumped elements of the proposed electrical circuit are extracted from the approximated rational function [25, 26]. The derived equivalent circuit is simulated in Advanced Design System (ADS) software. Measured and equivalent circuit model scattering parameters are perfectly matched. Finally, based on the formulated ECM of PIFA geometries with different stub lengths, the correlation between the equivalent circuit (EC) parameter values and the proposed open stub length is discussed in detail. The radiated power is also computed from the formed electric circuits of different PIFA geometries, having good agreement with the radiated power results obtained by full wave electromagnetic simulation in a High Frequency Structural Simulator (HFSS).

The detailed design and analysis of the proposed modification of PIFA structures with different open stub lengths, formulation of their electrical circuits, and the correlation between geometrical and EC parameters are discussed in the following sections.

II. Design and Analysis of Dual Band PIFA for Performance Enhancement

1. Modeling of the Proposed PIFA

The initial antenna model, which is used for modification to improve performance, is shown in Fig. 1. The antenna is a dual band PIFA (mostly used in modern cellular devices) having resonance frequencies in GSM 900 (low) and GSM 1800 (high) bands. The simulated model (Fig. 1) of the dual band PIFA depicts that it has a metallic IC near the antenna's radiating element. The width and height of the printed circuit board

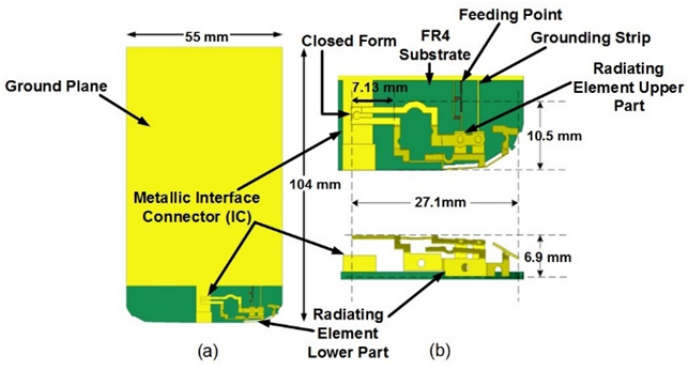

Fig. 1. Initial PIFA model: (a) Complete schematic, (b) antenna radiating structure with metallic interface connector.

(PCB) is 55 mm and 104 mm, respectively, which, in general, is the size of a low-cost 3.5-inch smart phone.

The metallic structure (antenna radiating element, IC, ground) is made of copper, and FR4 substrate is used as the dielectric below the antenna body. The EM analysis of the antenna model is performed in an HFSS. As illustrated in Fig. 1(b), the initial basic antenna radiating element is in the form of a closed loop at the top of a metallic IC. The presence of the metallic structure (IC) in close proximity to the antenna radiating element degrades the radiation properties of the PIFA. To reduce the effect of the IC on the radiation characteristics of the antenna and to improve the other performance metrics of the antenna, the addition of an open stub is proposed at the closed loop end of the PIFA structure. The modified antenna schematic is shown in Fig. 2. The proposed open stub reduces the length of the closed loop part.

The addition of an open stub in the PIFA structure shifts its radiating structure away from the metallic interface connector and ground plane. This shifting enhances the capacitive coupling with the reduction of the ground plane under the antenna radiator, as depicted in Fig. 3. An increase in the strong electric field region between the antenna radiator and the ground plane boosts the electrical volume of the antenna. The product of gain and bandwidth of an antenna has a direct relationship to the

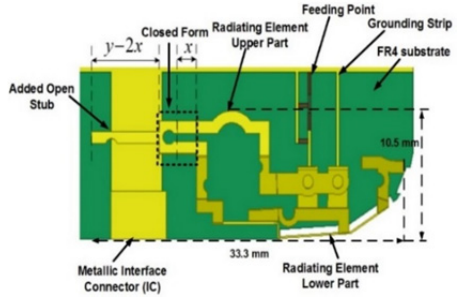

Fig. 2. The modified proposed PIFA structure with an added open stub.

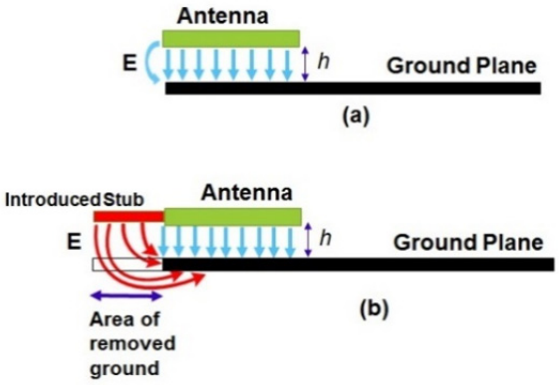

Fig. 3. Effect of introducing an open stub in the PIFA structure: (a) without stub, (b) with the proposed open stub.

antenna volume [27, 28]. The enhancement of the electrical volume of the PIFA with the addition of the proposed stub in its radiating structure increases its bandwidth and improves the return loss, gain, and efficiency characteristics.

2. Analysis of the PIFA with an Open Stub

In order to avoid any major changes in the resonance frequencies of the original PIFA, it is necessary to maintain the same total electrical lengths in the antenna models with and without the proposed open stub. The length of the open stub can be adjusted while keeping a constant relationship between the stub and the closed loop length. It has been observed through iterative simulations that the same optimum resonance performance of the old and modified PIFA can be obtained using the following simple relationship between the open stub and closed loop length:

$$l = y - 2x \tag{1}$$

In Eq. (1), l is the length of the proposed open stub, x is the length of the closed loop part, and y is the optimum length of the loop, which needs to be kept constant for the same resonance characteristics. A decrease of x means an increase in the stub length l. Fig. 2 illustrates Eq. (1). The lengths l and x can be varied, keeping y constant to obtain various PIFA models having identical resonances.

3. Simulation Results

Four PIFA models are made to show the effect of the added open stub length on various performance metrics. Simulated PIFA structures with various open stub lengths are shown in Fig. 4. Fig. 4(a), (b), (c), and (d) depict the PIFA geometries with stub lengths (l) of 0 mm, 2.8 mm, 6.8 mm, and 10.8 mm, respectively.

The predicted S_{11} results for all four cases are shown in Fig. 5. As indicated in Fig. 5, as the length of the proposed open

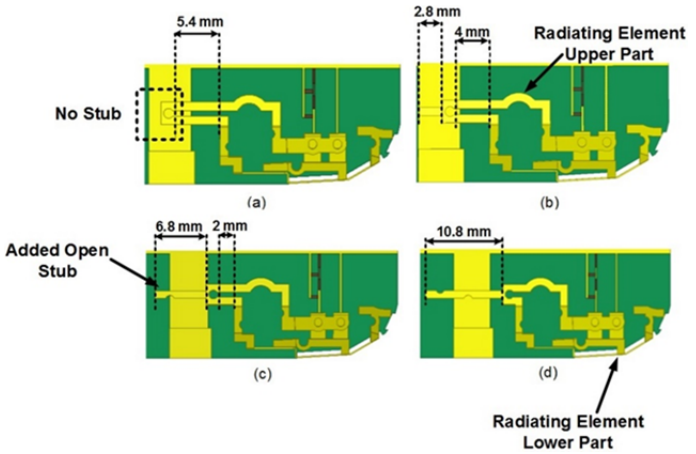

Fig. 4. Modified PIFAs: (a) $l = 0$ mm (no stub), (b) $l = 2.8$ mm, (c) $l = 6.8$ mm, and (d) $l = 10.8$ mm.

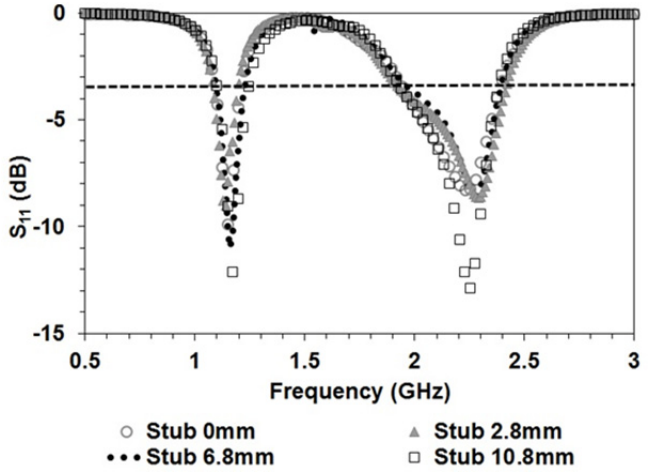

Fig. 5. Simulated S_{11} results for different lengths of open stubs: 0 mm (circle); 2.8 mm (shaded triangle); 6.8 mm (dotted line); and 10.8 mm (square).

stub (l) is gradually increased, the values of the scattering parameter show improvement. The reference used (VSWR ≤ 5) is an acceptable range for a commercial phone in the cellular industry. As shown in Table 1, 2.3 dB and 4.6 dB improvements in return loss are observed with a stub length of 10.8 mm in the lower and higher band PIFA models, and with $l = 10.8$ mm (Fig. 4(d)), maximum bandwidths of 130 MHz in the lower band (LB) and 440 MHz in the higher band (HB) are exhibited. The lower resonance band with a longer stub length PIFA geometry predicts a greater improvement in bandwidth as compared to the higher resonance band, and vice versa, for S_{11} characteristics.

Table 1. Comparison of predicted S_{11} and bandwidths (for VSW ≤5) in lower and higher bands with different stub lengths

Stub length l (mm)	Lower band		Higher band	
	Max. S_{11} (dB)	Bandwidth (MHz)	Max. S_{11} (dB)	Bandwidth (MHz)
0	−9.85	100	−8.31	430
2.8	−9.01	100	−8.65	470
6.8	−10.98	120	−8.54	410
10.8	−12.10	130	−12.88	440

4. Comparison of the Predicted and Measured Results

This section elaborates on the details of the performance of the fabricated PIFAs and its comparison with the simulated results. Dual band PIFA structures with stub lengths of 0 mm and 10.8 mm are fabricated and installed on actual cellular phones (Fig. 6). The metallic structure of the fabricated antennas is made of copper. The real PIFA geometries with stub lengths of 0 mm and 10.8 mm are shown in Fig. 6(b) and (c), respectively. Fig. 6 shows that the metallic IC is located in the vicinity of the radiating element of the actual antenna geometry.

The experimental setup for the S_{11} measurements of the fabricated antennas is illustrated in Fig. 7. Fig. 8 illustrates the correspondence of the predicted and experimental PIFA return losses with stub lengths of 0 mm and 10.8 mm, respectively.

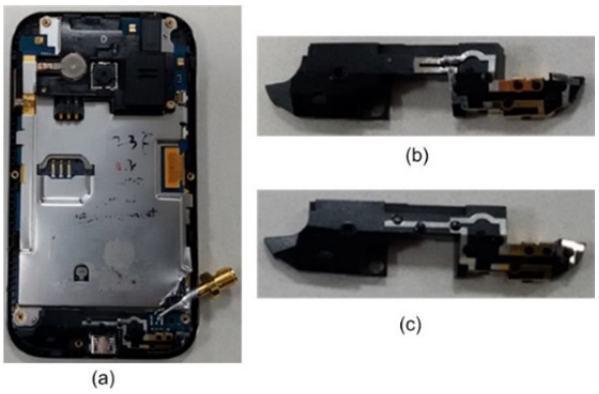

Fig. 6. Fabricated PIFA models: (a) complete PIFA model (l = 10.8 mm) installed on a cellular phone, (b) PIFA geometry with a stub length of 0 mm, and (c) PIFA geometry with a stub length of 10.8 mm.

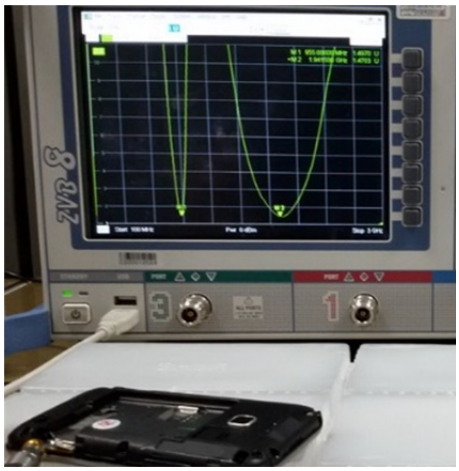

Fig. 7. Experimental setup for measurement of the scattering parameters of the PIFA models.

The simulated PIFA model includes only the PCB and the metallic IC of the actual mobile phone. However, in the actual measurements, the fabricated PIFA model is installed on a complete mobile phone set with a PCB, shield can, and various other modules. The possible reason the resonance frequency shifts in the measured results is because of the integration of the antenna on the complete mobile phone set. It is well known that the presence of various other metallic and non-metallic modules, such as a shield can, LCD of a mobile set, or camera, around an antenna in the vicinity of the PIFA radiating structure could change its resonance frequency in actual measurements. Note that in the simulation, we considered the antenna geometry only, not the materials around the antenna that are typically installed on a real mobile phone. As the methodology used for the development of the equivalent circuit proposed in this paper can be applied to any *S*-parameter data, we used the measured *S*-parameters instead of the simulated ones.

As indicated in Fig. 8, performance of the S_{11} parameters improved in the longer stub length structures. The maximum value return loss variations for the PIFAs are depicted in Fig. 9(a). Noticeable enhancements of 2.3 dB and 4.6 dB in the lower resonance band and 4.6 dB and 2 dB in the higher resonance band are observed for both the simulated and fabricated antennas, respectively. Fig. 9(b) shows the quantitative relationship between the simulated and measured bandwidths (for VSWR $\leq$5) of the PIFAs. The results show that 30% and 2.3% bandwidths of the PIFA (stub length = 10.8 mm) is enhanced in the simulation for the lower and higher bands, respectively. The same fabricated model improves the bandwidth performance by 16.7% in the lower resonance band and by 9.5% in the higher resonance band.

The measured radiation patterns for each of the manufactured antennas at lower and higher resonance frequencies (f_r) are shown in Fig. 10 and Fig. 11, respectively. Both figures confirm that the antennas have almost omnidirectional radiation patterns. It can be noted from Fig. 10 and Fig. 11 that there is no major change in radiation pattern shape in either the XZ or the XY plane with the addition of the proposed open stub in the PIFA radiating structure.

The directivity of the PIFA is calculated by approximating the measured radiation pattern as a finite sum over a spherical region [29]. The ratio of the measured gain and directivity indicates the efficiency of the antenna [29]. The correspondence between the measured peak gain (dBi) and the efficiencies of both manufactured antenna geometries is shown in Fig. 12. The modified antenna with a longer added stub length has a more improved gain and efficiency throughout the whole band as compared to the PIFA with no stub. In the modified antenna, a comprehensive improvement of up to 1.8 dBi in gain and 12.4% in efficiency is observed in the whole band.

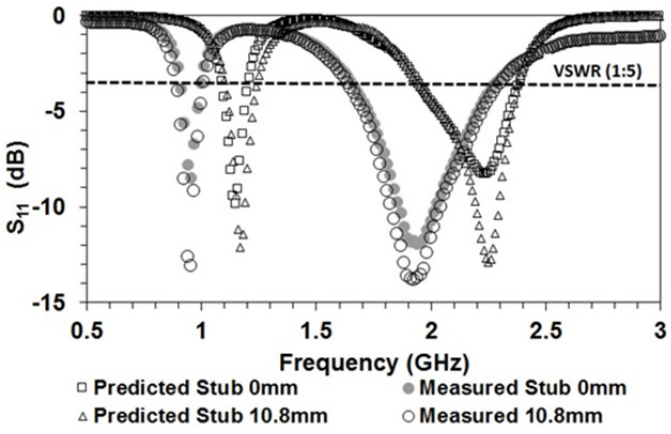

Fig. 8. Comparison of predicted and measured S_{11} with different stub lengths: predicted stub 0 mm (square), predicted stub 10.8 mm (rectangle), measured stub 0 mm (shaded circle), and measured stub 10.8 mm (circle).

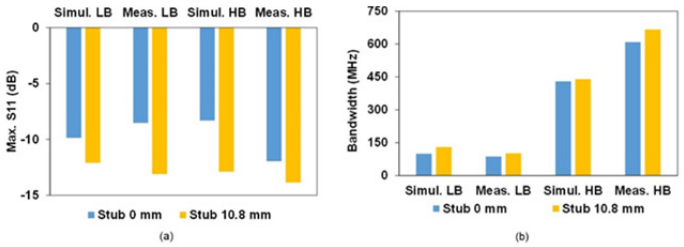

Fig. 9. Comparison of maximum return loss and bandwidth (for VSWR ≤5) with different stub lengths: (a) return loss, (b) bandwidth.

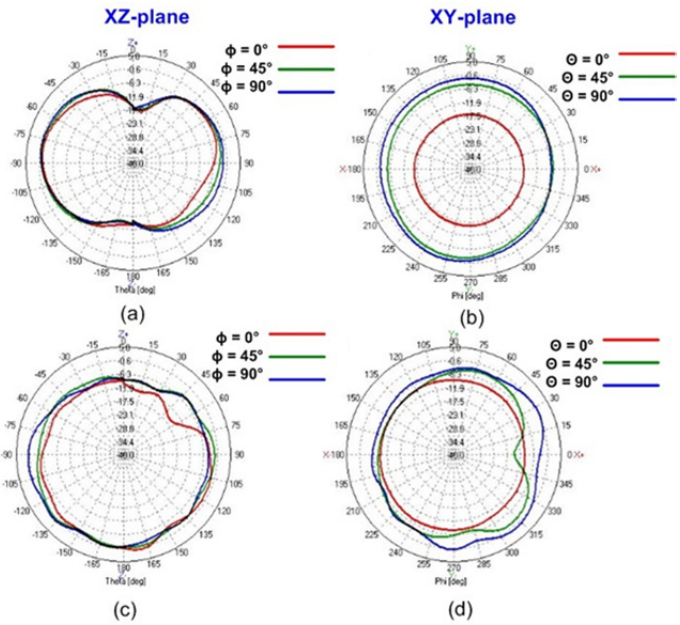

Fig. 10. Measured radiation pattern of 0 mm stub geometry: (a) XZ-plane at lower f_r, (b) XY-plane at lower f_r, (c) XZ-plane at higher f_r, and (d) XY-plane at higher f_r.

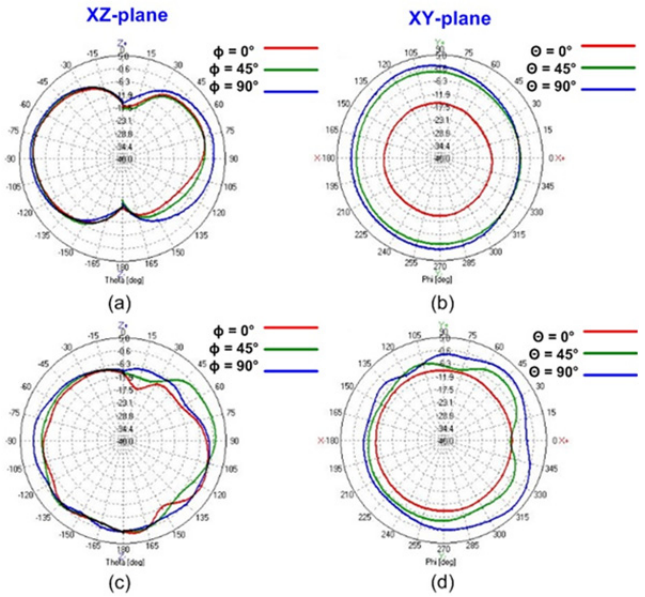

Fig. 11. Measured radiation pattern of 10.8 mm stub geometry: (a) XZ-plane at lower f_r, (b) XY-plane at lower f_r, (c) XZ-plane at higher f_r, and (d) XY-plane at higher f_r.

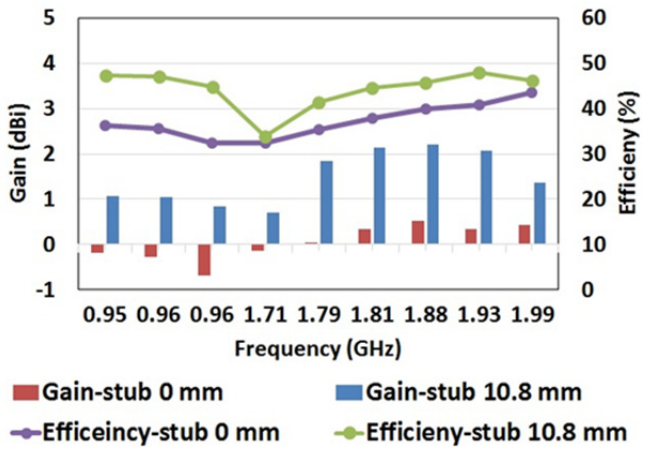

Fig. 12. Measured efficiency and gain of the fabricated antennas.

The simulated and measured S_{11}, measured radiation pattern, gain, and efficiency results for the fabricated and simulated antenna models confirm the noticeable enhancement in PIFA performance with the addition of an open stub in the PIFA structure. The used PIFA model geometry is extremely relevant to the conventional PIFA geometries used in the cellular phone industry. The proposed open stub is not in the way of the other active modules of the antenna, which makes it an effective and attractive solution from a practical implementation perspective. The correlation study and radiated power comparison of the formulation of the lumped equivalent circuits of the designed dual band PIFAs are discussed in the next section.

III. Lumped Equivalent Circuit Modeling of a Dual Band PIFA

An equivalent circuit model of the antenna is derived to illustrate the correlation between the lumped element values of the equivalent circuit and the proposed stub length in the PIFA structure. Step-by-step details of the proposed formulation of the lumped equivalent circuit of the dual band PIFA with a stub length of 10.8 mm is described in this section.

1. Rational Approximation of Frequency Response

The first step in the formulation of an equivalent circuit is the rational approximation of the predicted or measured frequency response data. Scattering/admittance parameters versus frequency data of the antenna model can be obtained through complete electromagnetic simulation using the Finite Element Method (FEM), the Finite-Difference Time Domain method (FDTD), the Transmission Line Model (TLM) method, or through hardware measurements. The obtained admittance data is approximated to rational functions using the widely applied vector fitting (VF) or pole fitting method [24, 26]. Vector fitting is a robust numerical technique that is used to convert frequency response data to rational functions. This technique is used for a wide range of microwave and electrical applications [24, 25, 30, 31]; here, it is used to approximate the measured admittance data of the dual band PIFA to Foster's canonical admittance rational form, Eq. (2). Foster's canonical admittance rational function [25, 30] $Y(s)$ of approximation is shown below:

$$Y(s)=\sum_{m=1}^{N}\frac{r_m}{s-\alpha_m}+d+e\cdot s \tag{2}$$

In Eq. (2), s is the single frequency point, r_m and α_m are the residuals and poles, respectively, N is the order of approximation, and d and e are higher order coefficients. The coefficients r_m and α_m can either be real or complex conjugate pairs while d and e are real. The order of approximation is equal to the number of poles. The aim is to find all r_m, α_m, and d and e in Eq. (2), so that the simulated/measured data can be represented in a rational form.

$Y(s)$ in Eq. (2) is the non-linear problem, as the poles are in the denominator. To covert this non-linear problem to a linear one so that it can be solved through linear square fitting and to start the fitting process, a set of initial poles $\{a_m\}$ are defined and Eq. (2) is multiplied by $\sigma(s)$.

$$\sigma(s)Y(s)=q(s) \tag{3}$$

where

$$\sigma(s)=1+\sum_{m=1}^{N}\frac{r_m}{s-a_m} \tag{4}$$

$$q(s)=\sum_{m=1}^{N}\frac{r_m}{s-a_m}+d+e.s \tag{5}$$

These initial poles (starting poles) are defined only at the starting point. The initial poles must have weak attenuation; the procedure and criteria for stating these initial poles is elaborated in [24]. It is shown that if Eq. (3) holds, then the poles of $Y(s)$ must be equal to the zeros of $\sigma(s)$ [24]. The new poles of $Y(s)$ are determined as the zeros of $\sigma(s)$, which are in fact the poles of $1/\sigma(s)$. The new poles are calculated as the eigenvalues in the following equation [24, 26]:

$$New\,poles\left\{a_m^{'}\right\}=Zeros\,of\;\sigma(\mathrm{s})=eig\left(A-bc^{T}\right) \tag{6}$$

In Eq. (6), A is a diagonal matrix with the initial poles $\{a_m\}$, b is a column vector of ones, and c^T is a row vector containing the residuals r'_m. The new set of poles $\left\{a_m^{'}\right\}$ replaces the initial poles in Eq. (3) after one iteration and the process of pole reallocation is repeated until convergence is achieved. The number of iterations depends on the fitting function and its convergence [24–30]. Once the poles are known, the coefficients r_m, d, and e are calculated by linearly solving the equation $Ax=B$ through singular value decomposition (SVD) [24–30] and the rational approximation of the frequency response is obtained. VF ensures the stability of the approximated rational function through pole-flipping to the left half plane [24, 26] and it also enforces the passivity of the model [32].

2. Synthesis of an Equivalent Circuit

The procedure used to extract the equivalent circuit component values from the approximated rational function is detailed in this section. The fitted $Y(s)$ in Eq. (2) shows that the network has branches between all nodes and grounds and between all nodes. It can be predicted from Eq. (2) that coefficients d and e are equal to the conductance and capacitor branch between node and ground, respectively, and their values can be calculated as

$$G_o=\frac{1}{R_o}=d\quad;\qquad C_o=e \tag{7}$$

The poles $\{\alpha_m\}$ of $Y(s)$ can either be real or a complex conjugate. Real poles correspond to real residuals $\{r_m\}$ and they represent a series RL branch, as depicted in Fig. 13. The component values of the series m^{th} RL branch can be calculated using the following expressions:

$$Y(s)_m=\frac{r_m}{s-\alpha_m}=\frac{1/L_m}{s+R_m/L_m} \tag{8}$$

$$L_m=\frac{1}{r_m}\;;R_m=-\alpha_m L_m=-\frac{\alpha_m}{r_m} \tag{9}$$

For complex conjugate poles pair $\{\alpha_m, \alpha'_m\}$, there is a relating complex conjugate residual coefficient $\{r_m, r'_m\}$, depicting a series RLCG network (Fig. 13). For this scenario, $Y(s)$ can be written as

$$Y(s)=\frac{r}{s-\alpha}+\frac{r'}{s-\alpha'}=\frac{a+jb}{s-(c+jd)}+\frac{a-jb}{s-(c-jd)} \tag{10}$$

$$Y(s)=\frac{2as-2(ac+bd)}{s^2-2cs+\left(c^2+d^2\right)} \tag{11}$$

For a generalized n^{th} complex pole conjugate pair (CPP) and residual branch, Eq. (11) can be written as

$$Y(s)_n=\frac{2\Re\{r_n\}s-2\Re\{r_n\alpha'_n\}}{s^2-2\Re\{\alpha_n\}s+|\alpha_n|^2} \tag{12}$$

Using the circuit network theory, the admittance of the n^{th} series RLCG branch can be expressed as

$$Y(s)_n=\frac{s(1/L_n)+G_{nc}/L_nC_n}{s^2+(R_n/L_n+G_{nc}/C_n)s+(R_nG_{nc}/L_nC_n+1/L_nC_n)} \tag{13}$$

Comparing Eq. (12) and Eq. (13), the following generalized formulas are obtained for each component of the n^{th} RLCG branch.

$$L_n=\frac{1}{2\Re\{r_n\}};\quad R_n=L_n\left(-2\Re\{\alpha_n\}+2L_n\Re\{r_n\alpha'_n\}\right) \tag{14}$$

$$C_n=\frac{1}{L_n\left(2R_n\Re\{r_n\alpha'_n\}+|\alpha_n|^2\right)} \tag{15}$$

$$G_n=\frac{1}{R'_n}=-2\Re\{r_n\alpha'_n\}L_nC_n \tag{16}$$

The element values of each branch of the series RLCG network can be computed using Eqs. (14)–(16). All branch elements are connected in parallel and the complete schematic of the synthesized equivalent circuit of Eq. (2) is shown in Fig. 13.

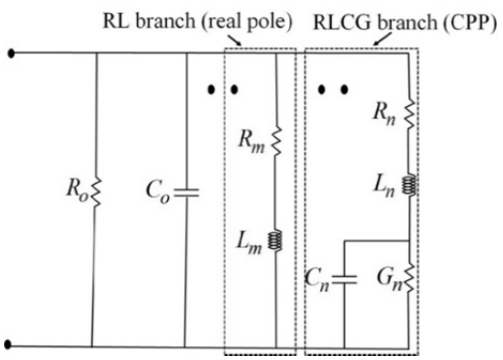

Fig. 13. Basic single port synthesized equivalent circuit schematic.

3. Rational Fitting of the Dual Band PIFA Frequency Response

The measured PIFA admittance data ($l = 10.8$ mm) has resonance frequencies of 0.955 GHz and 1.17 GHz and is fitted to a *12th* order approximation ($N = 12$) using the following starting poles: $-0.8e7 \pm j0.8e9$, $-1e7 \pm j1e9$, $-1.3e7 \pm j1.3e9$, $-1.4e7 \pm j1.4e9$, $-1.9e7 \pm j1.9e9$, and $-2.0e7 \pm j2.0e9$. The location of the starting poles depends upon the resonance frequencies of the measured/simulated input admittance/*S*-parameter data.

Lower orders of approximation of admittance data produce inaccurate results as at least two CPP are necessary for one resonance frequency for accurate fitting of data using VF. However, higher orders of approximation are unnecessary. The fitting process is carried out with three iterations and results in a root mean square (RMS) error of 3.46*e*-4. The approximated fitting rational function and the original measured admittance data magnitude and phase angle versus frequency results are depicted in Fig. 14(a) and (b), respectively. The magnitude and phase angle results of the approximated admittance rational function (Y_{fit}) and the original measured data (Y: input data) are in good agreement, as illustrated in Fig. 14(a) and (b).

4. Electrical Circuit of Dual Band PIFA

The *12th* order approximation of the frequency domain response produces six CPPs that correspond to six series RLCG branches, as well as one resistor ($R_o = 2.48\,\text{k}\Omega$) and one capacitor ($C_o = 0.36\,\text{pF}$) branch. The parameter values for each RLCG branch are calculated using Eqs. (14)–(16) and are depicted in Table 2. Fig. 15 shows the circuit model simulated in the ADS. The comparison of measured, fitted rational function, and equivalent circuit model S_{11} results is depicted in Fig. 16.

Although the produced equivalent circuit has some negative resistance elements, the overall response of the system is stable and converged as the VF ensures the passivity and stability of the approximated rational function with the shifting of unstable poles to the left-half plane [31, 32]. With the guaranteed stable poles and enforced passivity of the VF technique, the electrical simulation of the circuit will remain stable as the circuit on the whole will always consume power [32]. The number and values of the generated unphysical elements are dependent upon the order of approximation used for fitting and the frequency range of the approximated function. Lower orders of approximation will produce less negative components but it may increase the fitting RMS error. The negative resistance values can be converted to absolute values by using the procedure for resistance inversion described in [30] with the limitation of lower orders of fitting approximation.

The complete process for obtaining simulated/measured admittance data versus frequency, rational approximation of the input frequency response data, extraction of the lumped element parameter values of the equivalent circuit from the approximated rational function, and simulation of the formed equivalent circuit in a circuit simulator for the illustration of its scattering parameters are summarized in the form of a flowchart

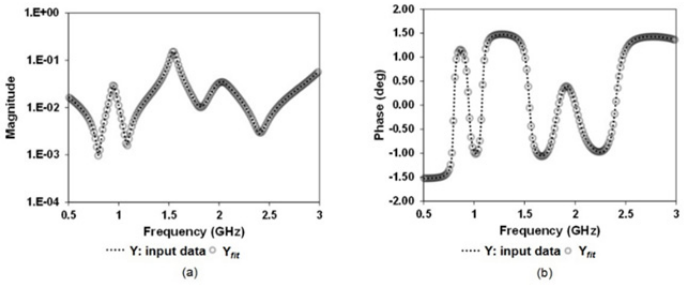

Fig. 14. Fitted rational function (Y_{fit}) and measured (Y: input data) admittance results: (a) magnitude, (b) phase.

Table 2. ECM RLCG parameters values for a dual band PIFA

	RLCG Br. 1	RLCG Br. 2	RLCG Br. 3	RLCG Br. 4	RLCG Br. 5	RLCG Br. 6
$R_n(\Omega)$	1.63	37.54	20.04	−16,431	30.88	3.11
L_n (nH)	13.58	107.59	16.48	−355.40	22.83	4.97
C_n (pF)	1,0004.77	0.262	0.63	−0.001	0.27	0.49
$R_n^{'}$(kΩ)	0.003	−100.13	−1.913	17.68	−63.92	−71.24

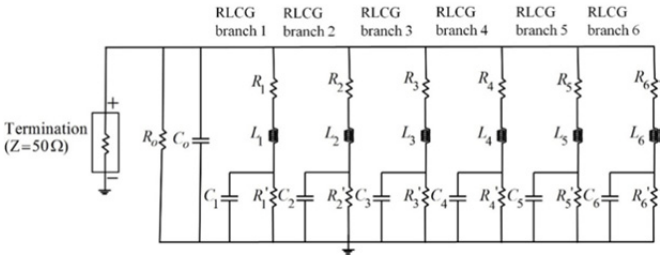

Fig. 15. ADS model of the developed electrical circuit for a dual band PIFA.

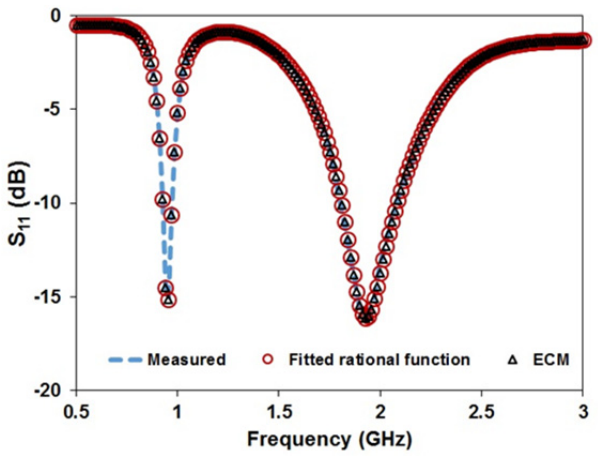

Fig. 16. Comparison of S_{11} results of the fabricated antenna, fitted rational function, and lumped equivalent circuit model.

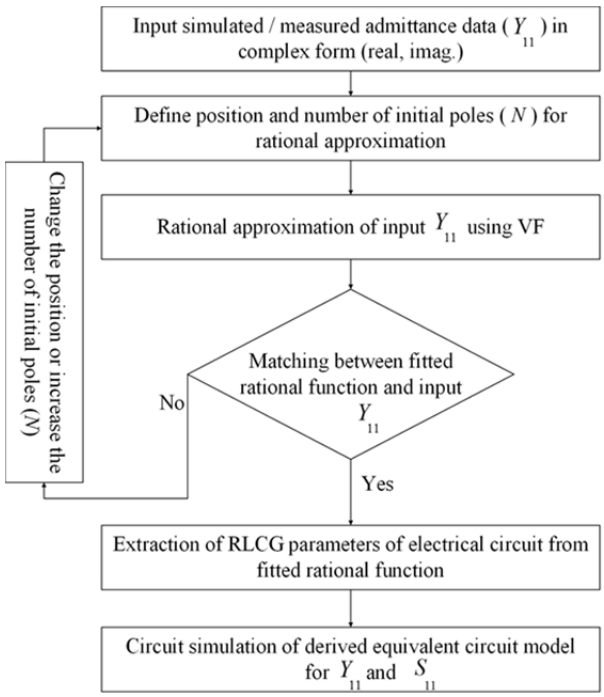

Fig. 17. Flowchart for equivalent circuit formulation.

in Fig. 17.

The proposed method for equivalent circuit formulation is quite simple and good agreement between the electrical circuit and simulated/measured results is obtained. An electrical model for single/multiband antennas can be predicted using the proposed methodology. This described method is used to illustrate the correlation between a PIFA's geometrical parameters and its respective equivalent circuit element values.

IV. Correlation between the Equivalent Circuit Parameters and the Physical Open Stub Length of Dual Band PIFAs

The effect of the proposed open stub length on the performance of dual band PIFAs and the formation of an equivalent circuit from the frequency response has been described in previous sections. Here, we present the study on the correlation between the formed equivalent circuit models of various PIFA geometries (with different stub lengths) and a comparison of the radiation power results.

1. EC Formulation of PIFAs with Different Stub Lengths

Rational approximation of the simulated frequency response of dual band PIFA geometries with stub lengths (l) of 0 mm, 2.8 mm, 6.8 mm, and 10.8 mm is performed using the procedure described in Fig. 17. The lumped equivalent circuits for each PIFA structure are extracted from their formed rational functions.

The simulated admittance data of PIFA geometry with $l=$ 2.8 mm and 10.8 mm produce the best fitting of rational function with four starting poles; consequently, the formulated ECM has four RLCG branches. The initial poles used for these geometries are $-0.9e7 \pm j0.9e9$, $-1.3e7 \pm j1.3e9$, $-2.1e7 \pm j2.1e9$, and $-2.3e7 \pm j2.3e9$. However, repeated simulations show that the more accurate equivalent circuits (less difference between the simulated [HFSS] and equivalent circuits S_{11}) of PIFAs with smaller stub lengths ($l=0$ mm and 6.8 mm) are obtained with six starting CPPs (12^{th} order approximation). Starting poles $-1.1e7 \pm j1.1e9$, $-1.2e7 \pm j1.2e9$, $-1.4e7 \pm j1.4e9$, $-1.6e7 \pm j1.6e9$, $-2.2e7 \pm j2.2e9$, and $-2.5e7 \pm j2.5e9$ are used for the admittance data fitting of both PIFAs ($l=0$ mm and 6.8 mm). Six RLCG branches along with R_o and C_o are obtained for the equivalent circuits of each PIFA with stub lengths of 0 mm and 6.8 mm, respectively. Rational approximation of all PIFA models is done using three iterations. PIFA geometries with stub lengths of 2.8 mm and 10.8 mm have smoother frequency responses than other PIFA structures ($l=0$ mm and 6.8 mm). That is why the best rational function fitting is obtained with a lower order of approximation (N).

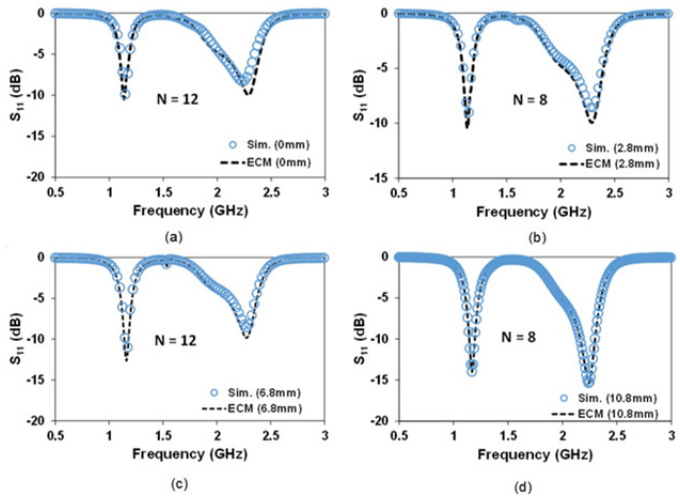

Fig. 18. Comparison of simulated and equivalent circuit return loss: (a) $l=0$ mm, (b) $l=2.8$ mm, (c) $l=6.8$ mm, and (d) $l=10.8$ mm.

Fig. 18 illustrates that the return loss of the simulated and produced equivalent circuits for each PIFA are in good agreement. The difference between the amplitude of the simulated frequency response and the approximated rational function in terms of RMS error is depicted in Fig. 19. All PIFA geometry fitted rational functions have RMS error values in the order of 1e-4. These values can be further reduced with higher orders of approximation; however, this is unnecessary as the RMS error is of a lower order and good frequency response fitting of the respective PIFA is obtained with the used order of approximation. An increase in order will consequently increase the number of RLCG branches, which seems unnecessary.

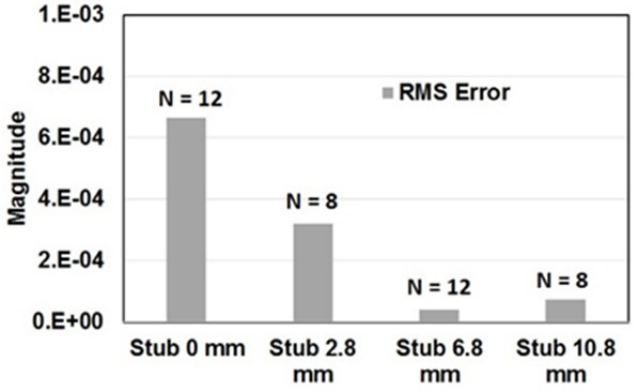

Fig. 19. Comparison of root mean square error of fitting for various PIFA structures.

2. Correlation between the EC Parameters of PIFAs with Different Stub Lengths

The details of the correlation between the computed EC parameters of PIFAs with different stub lengths is explained in this section. Fig. 20 illustrates the relationship between the parallel lumped element (R_o and C_o) branches of equivalent circuits for various PIFA geometries. As indicated in Fig. 20, PIFAs with smaller stub lengths have higher C_o branch values. The value of the parallel capacitor branch (Fig. 13) decreases with an increase in length of the open stub, and vice versa for parallel resistor R_o values.

Fig. 21 depicts the correlation between the element values of series RLCG branches of equivalent circuits for different PIFA geometries. The correspondence between the absolute values of the R_n and G_n of equivalent circuits for each respective PIFA is shown in Fig. 21(a), while Fig. 21(b) illustrates the relationship between the absolute value of L_n and C_n values. The ratios of G_n/R_n and C_n/L_n for all four formed equivalent circuits for each PIFA is almost constant, except for the first RLCG branch of each circuit. PIFAs with longer stub lengths (l) have higher G_n/R_n ratio values for the first RLCG branch formed by the first CPP; these values gradually decrease with increasing stub length. All higher order branches exhibit almost constant values for both G_n/R_n and C_n/L_n ratios,

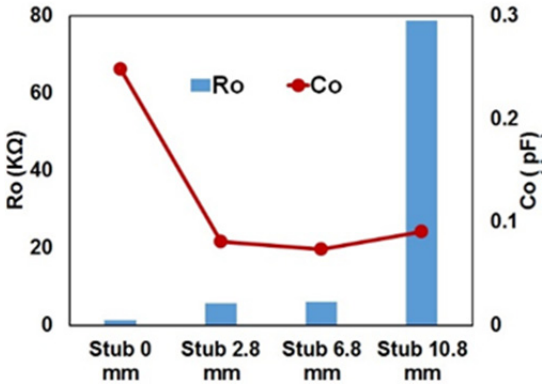

Fig. 20. Correlation between R_o, C_o for various PIFA structures.

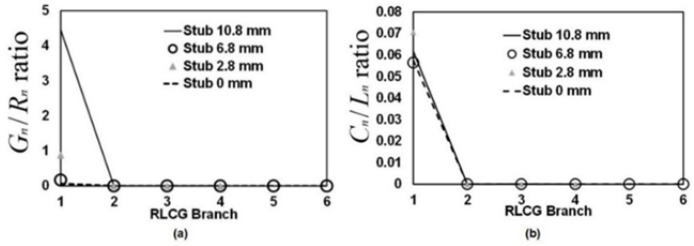

Fig. 21. Correlation between series RLCG values of EC for different PIFA structures.

with ratio values of the order 1*e*-5. Although the C_n/L_n ratio for the 2.8 mm stub structure increases for the first RLCG branch, the difference between the ratio values for the various equivalent circuits is very low.

As elaborated in Fig. 5, significant differences are not observed between the resonance frequencies of all four PIFA models. That is why the above stated ratios for the four equivalent circuits show similar behaviors. The presented correlation study suggests that for wider bandwidth and dipper return loss values for the designed PIFA, the R_o must be increased and the C_o component value must be decreased, with an almost constant relationship between theG_n/R_n and C_n/L_n ratios for the different RLCG branches (except for the first relating RLCG branch) of the equivalent circuit.

3. Electrical Circuit Radiated Power Estimation

The radiated power of an electrical circuit is dependent upon the power radiated by its resistive elements. The formed electrical circuit for dual band PIFAs in Section IV constitutes different numbers of resistive components (R_o, R_n, R_n') based on their order of approximation (N). The total number of resistive elements (N_{TR}) of an electrical circuit formulated using rational approximation can be computed using the following equation:

$$N_{TR} = N + 1 \tag{17}$$

In Eq. (17), N is the order of approximation of the vector fitting used for formation of the lumped equivalent circuit. For example, the number of resistive elements for an electrical circuit with $N = 8$ will be 9. The radiated power for each resistor is computed by dividing the square of the voltage drop across each resistive element by the resistance value. The computed radiated power for each resistive element is added to obtain the total radiated power of the lumped equivalent circuit. The total radiated power (RP_T) calculation formula for the electrical circuit is shown in Eq. (18).

$$RP_T = \sum_{i=1}^{N_{TR}} RP_i = \frac{1}{2}\sum_{i=1}^{N_{TR}} \frac{V_i^2}{R_i} \tag{18}$$

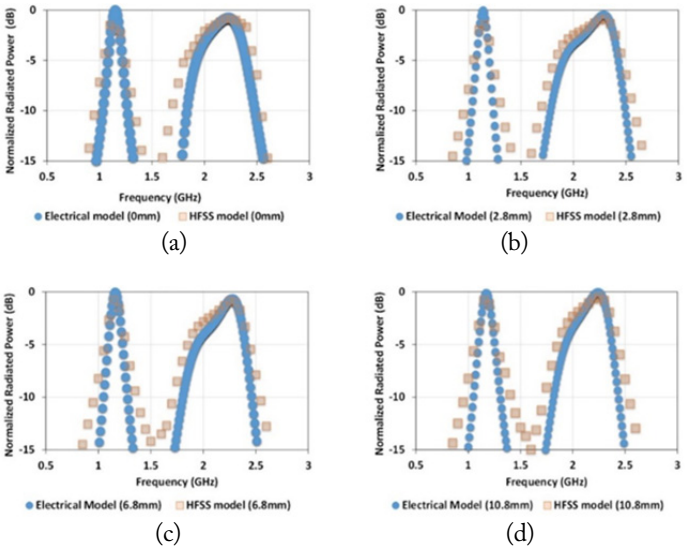

Fig. 22. Comparison of simulated and electrical circuit normalized radiated power: (a) $l=0$ mm, (b) $l=2.8$ mm, (c) $l=6.8$ mm, and (d) $l=10.8$ mm.

RP_i defines the computed radiated power of the i^{th} resistive element (R_i) of the electrical circuit having a voltage drop of V_i.

4. Comparison of Radiated Power Results

All the electrical models developed for the different PIFA geometries are simulated in an ADS circuit simulator for the calculations of radiated power from each electrical model using Eq. (18). In addition, the radiated power from the physical geometries of the PIFAs is calculated in an HFSS. A comparison of the radiated power from electrical circuits and the simulated HFSS models is shown in Fig. 22(a), (b), (c), and (d), which depict the results of normalized radiated power for PIFA structures with stub lengths of 0 mm, 2.8 mm, 6.8 mm, and 10.8 mm, respectively. It can be seen that the normalized radiated power results of the simulated PIFA geometries and the developed equivalent circuit models are in good agreement.

The presented results show that electrical circuits formed using the proposed methodology of rational fitting can be used to depict the various radiation characteristics of the antenna, which are closely related to the computed radiation properties, using a full wave electromagnetic simulation in much less time than the computation time required to complete simulation in EM software.

V. Advantages of the Proposed Methodology

The advantages of the proposed equivalent circuit modeling, correlation analysis, and radiated power computation are summarized as follows:

• The proposed method for ECM is easy and relatively simple. The techniques for ECM in the form of transmission line, RLC resonators, or using the (PEEC) method has certain limitations either in the form of antenna geometry or in that the number of lumped elements of the produced equivalent circuit are quite large (as in the produced SPICE equivalent circuit modeled by the PEEC technique) [19]. The agreement between the simulated/measured antenna and ECM return loss results is not good for the transmission line and RLC resonators techniques [14, 15]. The electric circuit produced using the proposed method has almost perfectly matched agreement between the electrical model and the fabricated/simulated PIFA geometry results.

• The ECM of the antenna is done for ease in systematically designing the PIFA model for bandwidth, gain, and efficiency enhancement using the equivalent lumped elements of the circuit. The good agreement between the radiated powers calculated from the electrical models and the actual PIFA geometries shows that the ECM can be used to analyze the various radiation characteristics of the actual antenna geometry. The presented approach offers the advantage of saving computation time in full wave EM simulation.

• The designed ECM can also be used for time domain analyses (such as transient behavior simulation) of circuits including PIFAs. If a circuit including a PIFA needs to be analyzed, the proposed electrical circuit would be the best model for predicting the overall circuit behavior. The presented correlation analysis between the PIFA geometry and electrical models would be useful for antenna designers who wish to enhance the performance of the PIFA and it contributes to its systematic design. The proposed method of electric circuit formulation has potential uses in advancing the understanding of various electromagnetic and microwave structures by analyzing the electrical performances of their equivalent circuits.

VI. Conclusion

This work presented a design, analysis, and simple method for the formulation of lumped equivalent circuit models for dual band PIFAs. The presence of a metallic interface connector around the PIFA radiating structure degrades its radiating power, return loss, and bandwidth performance. It has been shown that the addition of the proposed open stub to the PIFA geometry improves the various performance metrics of a PIFA. PIFA models with various open stub lengths were created to illustrate the effect of the length on PIFA performance, and it was found that the enhancement of PIFA characteristics was proportional to the stub length. The predicted and measured PIFA results confirm up to 4.6 dB, 17%, 2 dBi, and 12.4% improvements in return loss, bandwidth, gain, and efficiency values, respectively. The second presented work illustrates a simple procedure for the modeling of a lumped equivalent cir-

cuit for the designed dual band PIFAs. The measured/simulated admittance data for each PIFA geometry with different stub lengths were approximated to a rational function using a pole fitting method. Subsequently, a lumped equivalent circuit was formed and its element values were derived from the fitted rational functions of each geometry. The predicted/measured and formed equivalent circuit scattering parameters agreed extremely well. Finally, the correspondence between the physical stub length of various PIFA structures and their derived equivalent circuits was discussed in detail, which will be useful in the examination of the relationship between actual designed PIFA structures and their equivalent circuits.

This research was supported by the Basic Science Research Program through the National Research Foundation of Korea (NRF) funded by the Ministry of Science, ICT and Future Planning (No. NRF-2013R1A1A2009489).

References

[1] J. Anguera, A. Andujar, M. Huynh, C. Orlenius, C. Picher, and C. Puente, "Advances in antenna technology for wireless handheld devices," *International Journal of Antennas and Propagation*, vol. 2013, article no. 838364, pp. 1–25, 2013.

[2] K. L. Wong, *Planar Antennas for Wireless Communications*, New York: John Wiley & Sons, 2003.

[3] R. Hossa, A. Byndas, and M. Bialkowski, "Improvement of compact terminal antenna performance by incorporating open-end slots in ground plane," *IEEE Microwave and Wireless Components Letters*, vol. 14, no. 6, pp. 283–285, 2004.

[4] F. Yang, X. X. Zhang, X. Ye, and Y. Rahmat-Samii, "Wide-band E-shaped patch antennas for wireless communications," *IEEE Transactions on Antennas and Propagation*, vol. 49, no. 7, pp. 1094–1100, 2001.

[5] J. S. Kuo and K. L. Wong, "Dual-frequency operation of a planar inverted-L antenna with tapered patch width," *Microwave and Optical Technology Letters*, vol. 28, no. 2, pp. 126–127, 2001.

[6] K. L. Wong, *Compact and Broadband Microstrip Antennas*, New York: John Wiley & Sons, 2002.

[7] N. Firoozy and M. Shirazi, "Planar inverted-F antenna (PIFA) design dissection for cellular communication application," *Journal of Electromagnetic Analysis and Applications*, vol. 3, no. 10, pp. 406–411, 2011.

[8] J. Chun, J. Shim, and T. S. Kim, "Design of wideband cylindrical monopole antenna," *Journal of the Korean Institute of Electromagnetic Engineering and Science*, vol. 7, no. 2, pp. 69–73, 2007.

[9] C. Rowell and R. Murch, "A compact PIFA suitable for dual-frequency 900/1,800-MHz operation," *IEEE Transactions on Antennas and Propagation*, vol. 46, no. 4, pp. 596–598, 1998.

[10] J. H. Lu and K. L. Wong, "Slot-loaded, meandered rectangular microstrip antenna with compact dual frequency operation," *Electronics Letters*, vol. 34, no. 11, pp. 1048–1050, 1998.

[11] H. D. Chen, "Compact circularly polarised microstrip antenna with slotted ground plane," *Electronics Letters*, vol. 38, no. 13, pp. 616–617, 2002.

[12] T. Sugiyama, H. Horita, Y. Shirakawa, M. Ikegaya, S. Takaba, and H. Tate, "Triple-band internal antenna for clamshell type mobile phone," *Hitachi Cable Review*, no. 2, pp. 26–31, 2003.

[13] M. Salehi and M. Manteghi, "Transient characteristics of small antennas," *IEEE Transactions on Antennas and Propagation*, vol. 62, no. 5, pp. 2418–2429, 2014.

[14] M. Hamid and R. Hamid, "Equivalent circuit of dipole antenna of arbitrary length," *IEEE Transactions on Antennas and Propagation*, vol. 45, no. 11, pp. 1695–1696, 1997.

[15] Y. Liao, T. H. Hubing, and D. Su, "Equivalent circuit for dipole antennas in a lossy medium," *IEEE Transactions on Antennas and Propagation*, vol. 60, no. 8, pp. 3950–3953, 2012.

[16] J. P. Kim, "Network modeling and circuit characteristics of aperture coupled vertically mounted strip antenna," *Journal of the Korean Institute of Electromagnetic Engineering and Science*, vol. 11, no. 2, pp. 122–127, 2011.

[17] T. G. Tang, Q. M. Tieng, and M. W. Gunn, "Equivalent circuit of a dipole antenna using frequency-independent lumped elements," *IEEE Transactions on Antennas and Propagation*, vol. 41, no. 1, pp. 100–103, 1993.

[18] Y. Liao, K. Cai, T. H. Hubing, and X. Wang, "Equivalent circuit of normal mode helical antennas using frequency-independent lumped elements," *IEEE Transactions on Antennas and Propagation*, vol. 62, no. 11, pp. 5885–5888, 2014.

[19] R. Bhattacharya, S. Srikanth, R. Garg, and T. Bhattacharyya, "Physics-based compact lumped circuit model of PIFA using a retarded partial element equivalent circuit," in *Proceedings of IEEE Asia-Pacific Conference on Antennas and Propagation (APCAP)*, Singapore, 2012, pp. 315–316.

[20] K. Boyle and L. Ligthart, "Radiating and balanced mode analysis of PIFA antennas," *IEEE Transactions on Antennas and Propagation*, vol. 54, no. 1, pp. 231–237, 2006.

[21] Z. Qi, F. Kan, and T. Z. Liang, "Analysis of planar inverted-F antenna using equivalent models," in *Proceedings of IEEE Antennas and Propagation Society International*

Symposium, Washington, DC, 2005, pp. 142–145.

[22] S. C. Del Barrio, M. Pelosi, O. Franek, and G. Pedersen, "Equivalent circuit model of a high Q tunable PIFA," in *Proceedings of 2001 IEEE Vehicular Technology Conference*, San Francisco, CA, 2011, pp. 1–4.

[23] A. Cabedo, J. Anguera, C. Picher, M. Ribo, and C. Puente, "Multiband handset antenna combining a PIFA, slots, and ground plane modes," *IEEE Transactions on Antennas and Propagation*, vol. 57, no. 9, pp. 2526–2533, 2009.

[24] B. Gustavsen and A. Semlyen, "Rational approximation of frequency domain responses by vector fitting," *IEEE Transactions on Power Delivery*, vol. 14, no. 3, pp. 1052–1061, 1999.

[25] J. Yousaf, H. Jung, and W. Nah, "Equivalent circuit modeling of dual band PIFA using rational approximation," in *Proceedings of 2014 Korea-Japan Microwave Workshop*, Suwon, Korea, 2014, pp. 63–64.

[26] P. Russer, M. Righi, C. Eswarappa, and W. J. R. Hoefer, "Lumped element equivalent circuit parameter extraction of distributed microwave circuits via TLM simulation," in *Proceedings of IEEE MTT-S International Microwave Symposium Digest*, San Diego, CA, 1994, pp. 887–890.

[27] B. Gustavsen, "Computer code for rational approximation of frequency dependent admittance matrices," *IEEE Transactions on Power Delivery*, vol. 17, no. 4, pp. 1093–1098, 2002.

[28] M. Gustafsson, C. Sohl, and G. Kristensson, "Physical limitations on antennas of arbitrary shape," *Proceedings of the Royal Society of London A: Mathematical, Physical and Engineering Sciences*, vol. 463, no. 2086, pp. 2589–2607, 2007.

[29] R. F. Harrington, "Effect of antenna size on gain, bandwidth, and efficiency," *Journal of Research of the National Bureau of Standards*, vol. 64D, no. 1, pp. 1–12, 1960.

[30] *IEEE Standard Test Procedures for Antennas*, IEEE Standard 149-1979, 1979.

[31] G. R. DeJean and M. M. Tentzeris, "The application of lumped element equivalent circuits approach to the design of single-port microstrip antennas," *IEEE Transactions on Antennas and Propagation*, vol. 55, no. 9, pp. 2468–2472, 2007.

[32] M. M. M. Ali, A. A. R. Saad, and E. E. M. Khaled, "A design of miniaturized ultra-wideband printed slot antenna with 3.5/5.5 GHz dual band-notched characteristics: analysis and implementation," *Progress in Electromagnetics Research B*, vol. 52, pp. 37–56, 2013.

[33] B. Gustavsen and A. Semlyen, "Enforcing passivity for admittance matrices approximated by rational functions," *IEEE Transactions on Power Systems*, vol. 16, no. 1, pp. 97–104, 2001.

Jawad Yousaf

received his B.S. degree in Communication Systems Engineering from the Institute of Space Technology, Islamabad, Pakistan, in 2009 and his M.S degree in Electrical and Electronics Engineering from Sungkyunkwan University, Suwon, Korea, in 2016. He is currently working toward a Ph.D. at the School of Electrical and Electronics Engineering at Sungkyunkwan University. His research interests include antenna design and modeling, electromagnetic interference/electromagnetic compatibility measurements of systems for space and commercial environments, and electrostatic discharge.

Hojin Jung

received his B.S. and M.S degrees in Electrical and Electronics Engineering from Ajou University and Sungkyunkwan University, Suwon, Korea, in 2005 and 2014, respectively. He has been working for Samsung Electronics as an RF engineer for 12 years. His research interests include antenna design and RF systems for mobile phones. His current research involves antenna design and performance improvement of radiation in mobile phones for the Chinese market.

Kwangho Kim

received his B.S. and M.S. degrees in Electrical and Electronics Engineering from Sungkyunkwan University, Suwon, Korea, in 2013 and 2015, respectively. He is currently enrolled in the Ph.D. candidate course in the School of Electrical and Electronics Engineering at Sungkyunkwan University. His research interests include the accuracy of high frequency measurements and system-level electromagnetic interference/electromagnetic compatibility. His current research topic focuses on the diagnosis of electrical components based on high frequency analysis such as power/control cables and transformers.

Wansoo Nah

received his Ph.D. in Electrical Engineering from Seoul National University, Korea, in 1991. He then joined the Korea Electrical Research Institute (KERI) as a senior researcher and was also a guest researcher at the Superconducting Super Collider Laboratory in the USA for about two years. He has been a professor at the College of Information and Communication Engineering at Sungkyunkwan University, Korea, since 1995. His present areas of interest include the analysis of signal integrity and power integrity, and the field of electromagnetic interference/electromagnetic compatibility.